UC Davis
UC Davis Previously Published Works

Title

Identifying Pythagorean-Hodograph Curves Closest to Prescribed Planar Bézier Curves

Permalink

https://escholarship.org/uc/item/30z6h57d

Author

Farouki, Rida T

Publication Date

2022-08-01

DOI

10.1016/j.cad.2022.103266

Peer reviewed

Identifying Pythagorean–hodograph curves closest to prescribed planar Bézier curves

Rida T. Farouki

Department of Mechanical and Aerospace Engineering,
University of California, Davis, CA 95616, USA.

Abstract

The problem of identifying the planar Pythagorean–hodograph curve
that is "closest" to a given Bézier curve, and has the same end points
(or end points and tangents), is considered. The "closeness" measure
employed in this context is the root–mean–square magnitude of the
differences between pairs of corresponding control points for the two
curves. The methodology is developed in the context of quintic PH
curves, although it readily generalizes to PH curves of higher degree.
Using the complex representation for planar curves, it is shown that
this problem can be reduced to the minimization of a quartic penalty
function in certain real variables, subject to two quadratic constraints,
which can be efficiently solved by the Lagrange multiplier method. By
expressing the penalty function and constraints in terms of variables
that identify a complex pre–image polynomial, the closest solution is
guaranteed to be a PH curve. Several computed examples are used to
illustrate implementation of the optimization methodology and typical
approximation results that can be obtained.

e–mail: farouki@ucdavis.edu

1 Introduction

The Pythagorean–hodograph (PH) curves are a family of parametric curves incorporating special algebraic structures that offer significant computational advantages over "ordinary" polynomial/rational parametric curves — these include exact measurement of arc length, rational offsets (for planar curves), and rational rotation–minimizing or minimal–twist frames (for spatial curves), among many others. For a more comprehensive treatment of the construction and properties of PH curves, the reader may consult [5, 9, 19].

Although PH curves are compatible with the standard Bézier/B–spline representations of modern CAD systems, they cannot be directly constructed and manipulated by the standard control–polygon methodology associated with those representations. Consequently, the primary means of constructing them has been by Hermite or spline interpolation of discrete data [2, 6, 7, 10, 11, 12, 15, 16, 21, 25]. An important result concerning the shape flexibility of PH curves is a Weierstrass–type approximation theorem [3], which shows that any given planar or spatial C^1 curve can be approximated to a prescribed accuracy by PH curves of a sufficiently high degree.

There have been several prior approaches to defining PH curves by control polygons. In [23] the C^2 planar PH quintic spline associated with a given knot sequence, end conditions, and control points, was identified as the "good" C^2 PH spline interpolant to the nodal points of the ordinary C^2 cubic B–spline specified by the same data. Subsequently, the problem of locally modifying C^2 planar PH quintic spline curves — while preserving their PH nature — was addressed in [8]. The concept of specifying PH curves through "rectifying" control polygons has been introduced and further developed in [17, 18, 22]. These are characterized by a number of control points that reflects the shape freedoms of PH curves of any given degree, and control polygon lengths that coincide with the total arc lengths of those PH curves.

The present study develops a novel approach to constructing planar PH curves based on identifying, for a given planar Bézier curve, the "closest" PH curve of related degree. The measure of closeness employed in this context is based on the sum of squared distances between corresponding control points of the two curves. Determination of the closest PH curve amounts to solving a non–linear constrained optimization problem, which is efficiently achieved through Newton–Raphson iterations in the context of the Lagrange multiplier method. This "closest PH curve" paradigm may be preferable to constructing PH curves by interpolation of discrete data when it is desired to replace an

existing set of polynomial curve segments by PH curve segments.

The methodology presented herein is closely related to a scheme presented in [1], which employs a constrained optimization approach to determine the PH B–spline curve whose control points are as close as possible to those of a prescribed "ordinary" B–spline curve. The focus herein is on the closeness of individual PH and Bézier curve segments, and the optimization variables, objective functions, and constraint equations are explicitly derived for low–degree cases of practical interest, to facilitate first–principles implementation. The computed examples provide an indication of the efficiency and accuracy attainable for individual curve PH and Bézier curve segments.

The plan for the remainder of this paper is as follows. Section 2 briefly reviews the complex–variable model for planar PH curves, and some of their advantageous computational properties. The identification of the PH curve closest to a given planar polynomial curve is then formulated as a constrained optimization problem in Section 3, with a particular focus on the quintic PH curves. Section 4 then illustrates an implementation of the method through some representative computed examples. Finally, some possible extensions and generalizations of the methodology are briefly outlined in Section 5, and Section 6 recapitulates the main contributions of this study.

2 Planar Pythagorean–hodograph curves

A planar polynomial PH curve $\mathbf{r}(t) = (x(t), y(t))$ is characterized by the fact that its derivative $\mathbf{r}'(t) = (x'(t), y'(t))$ has components satisfying [14] the Pythagorean condition

$$x'^2(t) + y'^2(t) = \sigma^2(t) \tag{1}$$

for some polynomial $\sigma(t)$, which defines the *parametric speed* of $\mathbf{r}(t)$, i.e., the derivative $\mathrm{d}s/\mathrm{d}t$ of arc length s with respect to the curve parameter t. The fact that $\sigma(t)$ is a polynomial (rather than the square root of a polynomial) endows PH curves with several attractive computational properties.

For a primitive curve $\mathbf{r}(t)$ with $\gcd(x'(t), y'(t)) = \text{constant}$, a sufficient and necessary condition for satisfaction of (1) is that $x'(t)$ and $y'(t)$ must be expressible [20] in terms of two polynomials $u(t), v(t)$ with $\gcd(u(t), v(t)) = \text{constant}$ as

$$x'(t) = u^2(t) - v^2(t), \quad y'(t) = 2\,u(t)v(t).$$

This structure is embodied in the complex representation [4], wherein a PH curve of degree $n = 2m+1$ is generated from a degree–m complex polynomial

$$\mathbf{w}(t) = u(t) + \mathrm{i}\, v(t) = \sum_{k=0}^{m} \mathbf{w}_k \binom{m}{k} (1-t)^{m-k} t^k \tag{2}$$

with Bernstein coefficients $\mathbf{w}_k = u_k + \mathrm{i}\, v_k$ by integration of the expression

$$\mathbf{r}'(t) = \mathbf{w}^2(t). \tag{3}$$

Because the parametric speed $\sigma(t) = |\mathbf{w}(t)|^2$ is a polynomial, the cumulative arc length function

$$s(t) = \int_0^t \sigma(\xi)\,\mathrm{d}\xi$$

is also a polynomial in t. Moreover, the unit tangent, normal, and curvature of $\mathbf{r}(t)$ are rational functions of t, specified [4] by

$$\mathbf{t}(t) = \frac{\mathbf{w}^2(t)}{\sigma(t)}, \quad \mathbf{n}(t) = \mathbf{t}(t) \times \mathbf{z}, \quad \kappa(t) = 2\,\frac{\mathrm{Im}(\overline{\mathbf{w}}(t)\mathbf{w}'(t))}{\sigma^2(t)}, \tag{4}$$

where $\mathbf{z}$ is a unit vector orthogonal to the plane, are all rational functions of t. Consequently, the offset curves

$$\mathbf{r}_d(t) = \mathbf{r}(t) + d\,\mathbf{n}(t)$$

at each distance d can be exactly represented as rational curves.

We focus here on quintic PH curves, since they are known [5] to possess sufficient shape freedoms for free–from design applications. The methodology can be readily extended to other contexts, although it is more cumbersome for PH curves of higher degree. A quintic PH curve $\mathbf{r}(t)$ may be generated by substituting a quadratic complex polynomial

$$\mathbf{w}(t) = \mathbf{w}_0(1-t)^2 + \mathbf{w}_1 2(1-t)t + \mathbf{w}_2 t^2 \tag{5}$$

into (3) and integrating. The control points of the Bézier representation

$$\mathbf{r}(t) = \sum_{k=0}^{5} \mathbf{p}_k \binom{5}{k} (1-t)^{5-k} t^k$$

3

are then determined from the coefficients $\mathbf{w}_0, \mathbf{w}_1, \mathbf{w}_2$ as

$$
\begin{aligned}
\mathbf{p}_1 &= \mathbf{p}_0 + \frac{1}{5}\,\mathbf{w}_0^2\,, \\
\mathbf{p}_2 &= \mathbf{p}_1 + \frac{1}{5}\,\mathbf{w}_0\mathbf{w}_1\,, \\
\mathbf{p}_3 &= \mathbf{p}_2 + \frac{1}{5}\,\frac{2\,\mathbf{w}_1^2 + \mathbf{w}_0\mathbf{w}_2}{3}\,, \\
\mathbf{p}_4 &= \mathbf{p}_3 + \frac{1}{5}\,\mathbf{w}_1\mathbf{w}_2\,, \\
\mathbf{p}_5 &= \mathbf{p}_4 + \frac{1}{5}\,\mathbf{w}_2^2\,,
\end{aligned}
\tag{6}
$$

with $\mathbf{p}_0$ being freely chosen. The end–point derivatives of $\mathbf{r}(t)$ are $\mathbf{r}'(0) = \mathbf{w}_0^2$ and $\mathbf{r}'(1) = \mathbf{w}_2^2$, and the end–point curvatures are $\kappa(0) = 4\,\mathrm{Im}(\overline{\mathbf{w}}_0\mathbf{w}_1)/|\mathbf{w}_0|^4$ and $\kappa(1) = 4\,\mathrm{Im}(\overline{\mathbf{w}}_1\mathbf{w}_2)/|\mathbf{w}_2|^4$.

3 Constrained optimization problem

Based on a suitable measure of "closeness," the task of identifying the planar PH curve $\mathbf{r}(t)$ closest to a prescribed Bézier curve $\mathbf{q}(t)$ can be formulated as a constrained polynomial optimization problem. The objective function and constraints may be expressed in terms of the coefficients of the pre–image polynomial (2) of $\mathbf{r}(t)$ and constants determined by the control points of $\mathbf{q}(t)$.

It is advantageous to use the complex representation [4] of planar Bézier curves and planar PH curves, wherein control points are regarded as complex values. Since ordinary Bézier cubics and planar PH quintics are both defined by four complex values — the four control points of the former, and the initial control point and three coefficients of the pre–image polynomial (5) for the latter — they have similar shape freedom, and it is natural to commence by identifying the planar PH quintic closest to a given planar Bézier cubic.

For brevity, we consider curves in *canonical form,* whose initial and final points coincide with the values 0 and 1 on the real axis. A plane curve can be mapped to canonical form by a translation/rotation/scaling transformation, and can be mapped back to its original position, orientation, and scale by the inverse of that transformation. A canonical–form PH quintic $\mathbf{r}(t)$ must satisfy the condition

$$
\int_0^1 \mathbf{r}'(t)\,\mathrm{d}t \;=\; \int_0^1 \mathbf{w}^2(t)\,\mathrm{d}t \;=\; \mathbf{r}(1) - \mathbf{r}(0) \;=\; 1\,.
$$

4

Substituting (5) and evaluating the integral yields a quadratic constraint on the complex coefficients $\mathbf{w}_0, \mathbf{w}_1, \mathbf{w}_2$ of (5) — namely,

$$2\,\mathbf{w}_1^2 + 3\,(\mathbf{w}_0 + \mathbf{w}_2)\mathbf{w}_1 + 3\,(\mathbf{w}_0^2 + \mathbf{w}_2^2) + \mathbf{w}_0\mathbf{w}_2 - 15 \;=\; 0\,. \tag{7}$$

In identifying the PH curve $\mathbf{r}(t)$ closest to a given ordinary planar Bézier curve $\mathbf{q}(t)$, it is desirable to impose end conditions on $\mathbf{r}(t)$. At minimum, we will require coincident end points — i.e., $\mathbf{r}(0) = \mathbf{q}(0)$ and $\mathbf{r}(1) = \mathbf{q}(1)$. In the context of smoothly joined curve segments, coincidence of the end tangents may also be required. Both theses cases are treated below. However, as more end constraints are imposed, the number of free parameters available in the optimization problem diminishes, and consequently the closeness of the PH curve to the given Bézier curve will generally be reduced.

3.1 G^0 PH quintic closest to an ordinary cubic

Consider a planar cubic Bézier curve given in canonical form,

$$\mathbf{q}(t) \;=\; \sum_{k=0}^{3} \mathbf{c}_k \binom{3}{k} (1-t)^{3-k} t^k\,, \tag{8}$$

whose control points satisfy $\mathbf{c}_0 = 0$ and $\mathbf{c}_3 = 1$. The first step is to elevate the degree of $\mathbf{q}(t)$ from 3 to 5, which results in the representation

$$\mathbf{q}(t) \;=\; \sum_{k=0}^{5} \mathbf{q}_k \binom{5}{k} (1-t)^{5-k} t^k\,, \tag{9}$$

with control points $\mathbf{q}_k = x_k + \mathrm{i}\,y_k$ given by

$$\mathbf{q}_0 \;=\; \mathbf{c}_0\,, \quad \mathbf{q}_1 \;=\; \frac{2\,\mathbf{c}_0 + 3\,\mathbf{c}_1}{5}\,, \quad \mathbf{q}_2 \;=\; \frac{\mathbf{c}_0 + 6\,\mathbf{c}_1 + 3\,\mathbf{c}_2}{10}\,,$$

$$\mathbf{q}_3 \;=\; \frac{3\,\mathbf{c}_1 + 6\,\mathbf{c}_2 + \mathbf{c}_3}{10}\,, \quad \mathbf{q}_4 \;=\; \frac{3\,\mathbf{c}_2 + 2\,\mathbf{c}_3}{5}\,, \quad \mathbf{q}_5 \;=\; \mathbf{c}_3\,.$$

We want to identify the quintic PH curve $\mathbf{r}(t)$ with control points $\mathbf{p}_0, \ldots, \mathbf{p}_5$ "closest" to $\mathbf{q}(t)$ that has the same end points. The control points of $\mathbf{r}(t)$ are expressed in terms of perturbations

$$\mathbf{p}_k \;=\; \mathbf{q}_k + \delta\mathbf{q}_k\,, \quad k = 0, \ldots, 5\,, \tag{10}$$

5

to the control points of $\mathbf{q}(t)$, such that $\mathbf{p}_0, \ldots, \mathbf{p}_5$ satisfy the relations (6) for some complex values $\mathbf{w}_0, \mathbf{w}_1, \mathbf{w}_2$. Choosing $\delta\mathbf{q}_0 = \delta\mathbf{q}_5 = 0$ guarantees that the end points of $\mathbf{r}(t)$ are coincident with those of $\mathbf{q}(t)$.

With $\delta\mathbf{q}_0 = \delta\mathbf{q}_5 = 0$, we define the measure of "closeness" of $\mathbf{r}(t)$ to $\mathbf{q}(t)$ by the quantity

$$\Delta = |\delta\mathbf{q}_1|^2 + |\delta\mathbf{q}_2|^2 + |\delta\mathbf{q}_3|^2 + |\delta\mathbf{q}_4|^2, \tag{11}$$

and observe that $\Delta = 0$ if and only if $\mathbf{q}(t)$ is itself a quintic PH curve. From (6) and (10) with $\delta\mathbf{q}_0 = \delta\mathbf{q}_5 = 0$ so that $\mathbf{q}_0 = \mathbf{p}_0 = 0$ and $\mathbf{q}_5 = \mathbf{p}_5 = 1$, the perturbations $\delta\mathbf{q}_1, \delta\mathbf{q}_2, \delta\mathbf{q}_3, \delta\mathbf{q}_4$ must be expressible in terms of the known control points of $\mathbf{q}(t)$ and three complex values $\mathbf{w}_0, \mathbf{w}_1, \mathbf{w}_2$ in the form

$$\delta\mathbf{q}_1 = \frac{1}{5}\mathbf{w}_0^2 - \mathbf{q}_1,$$

$$\delta\mathbf{q}_2 = \frac{1}{5}\mathbf{w}_0(\mathbf{w}_0 + \mathbf{w}_1) - \mathbf{q}_2,$$

$$\delta\mathbf{q}_3 = 1 - \frac{1}{5}(\mathbf{w}_1 + \mathbf{w}_2)\mathbf{w}_2 - \mathbf{q}_3,$$

$$\delta\mathbf{q}_4 = 1 - \frac{1}{5}\mathbf{w}_2^2 - \mathbf{q}_4. \tag{12}$$

Thus, the quintic PH curve closest to a given "ordinary" cubic Bézier curve $\mathbf{q}(t)$, with the same end points, is identified by substituting (12) into (11) and minimizing Δ with respect to $\mathbf{w}_0, \mathbf{w}_1, \mathbf{w}_2$ subject to the constraint (7). Substituting (12) into (11), simplifying, omitting terms that do not depend on $\mathbf{w}_0, \mathbf{w}_1, \mathbf{w}_2$, using the relation $|\mathbf{a}-\mathbf{b}|^2 = |\mathbf{a}|^2 + |\mathbf{b}|^2 - 2\operatorname{Re}(\mathbf{a}\,\bar{\mathbf{b}})$ for complex values $\mathbf{a}$ and $\mathbf{b}$, and scaling, we obtain the reduced form

$$\begin{aligned}\Delta =\ & |\mathbf{w}_0|^4 + |\mathbf{w}_0|^2\,|\mathbf{w}_0 + \mathbf{w}_1|^2 + |\mathbf{w}_1 + \mathbf{w}_2|^2\,|\mathbf{w}_2|^2 + |\mathbf{w}_2|^4 \\ & - 10\operatorname{Re}(\mathbf{w}_0^2\bar{\mathbf{q}}_1 + \mathbf{w}_0(\mathbf{w}_0 + \mathbf{w}_1)\bar{\mathbf{q}}_2 + (\mathbf{w}_1 + \mathbf{w}_2)\mathbf{w}_2(1 - \bar{\mathbf{q}}_3) + \mathbf{w}_2^2(1 - \bar{\mathbf{q}}_4))\end{aligned}$$

of (11), where $\bar{\mathbf{q}}_1, \bar{\mathbf{q}}_2, \bar{\mathbf{q}}_3, \bar{\mathbf{q}}_4$ are the complex conjugates of $\mathbf{q}_1, \mathbf{q}_2, \mathbf{q}_3, \mathbf{q}_4$.

Writing $\mathbf{w}_k = u_k + \mathrm{i}\,v_k$ for $k = 0, 1, 2$ the reduced objective function Δ depends on the six real variables[1] $u_0, v_0, u_1, v_1, u_2, v_2$ that are subject to two constraints — the real and imaginary parts of (7). Employing the Lagrange

---

[1]Since the modulus $|\mathbf{z}|$ of a complex number is not an analytic function of $\mathbf{z}$, the problem must be expressed in terms of real variables and equations to utilize optimization methods that employ derivatives.

multiplier method [26] for constrained optimization problems then yields a system of 8 real equations in 8 real unknowns — $u_0, v_0, u_1, v_1, u_2, v_2$ and the multipliers associated with the real and imaginary parts of (7).

The real and imaginary parts of the contraint equation (7) can be written as $g(u_0, v_0, u_1, v_1, u_2, v_2) = 0$ and $h(u_0, v_0, u_1, v_1, u_2, v_2) = 0$, where

$$
\begin{aligned}
g \;:=\; & 2\left(u_1^2 - v_1^2\right) + 3\left(u_0 u_1 - v_0 v_1\right) + 3\left(u_1 u_2 - v_1 v_2\right) \\
& + 3\left(u_0^2 - v_0^2\right) + 3\left(u_2^2 - v_2^2\right) + u_0 u_2 - v_0 v_2 - 15 \,,
\end{aligned}
\tag{13}
$$

$$
\begin{aligned}
h \;:=\; & 4\,u_1 v_1 + 3\left(u_0 v_1 + u_1 v_0\right) + 3\left(u_1 v_2 + u_2 v_1\right) \\
& + 6\,u_0 v_0 + 6\,u_2 v_2 + u_0 v_2 + u_2 v_0 \,,
\end{aligned}
\tag{14}
$$

and the objective function is

$$
\begin{aligned}
\Delta \;=\; & \left(u_0^2 + v_0^2\right)\left[\,2\left(u_0^2 + v_0^2\right) + u_1^2 + v_1^2 + 2\left(u_0 u_1 + v_0 v_1\right)\right] \\
& + \left(u_2^2 + v_2^2\right)\left[\,2\left(u_2^2 + v_2^2\right) + u_1^2 + v_1^2 + 2\left(u_1 u_2 + v_1 v_2\right)\right] \\
& - 10\left[\,(u_0^2 - v_0^2)(x_1 + x_2) + 2\,u_0 v_0(y_1 + y_2)\right] \\
& - 10\left[\,(u_0 u_1 - v_0 v_1)\,x_2 + (u_0 v_1 + u_1 v_0)\,y_2\right] \\
& - 10\left[\,(u_2^2 - v_2^2)(2 - x_3 - x_4) - 2\,u_2 v_2(y_3 + y_4)\right] \\
& - 10\left[\,(u_1 u_2 - v_1 v_2)(1 - x_3) - (u_1 v_2 + u_2 v_1)\,y_3\right].
\end{aligned}
\tag{15}
$$

The goal is to minimize the function (15) of the variables $u_0, v_0, u_1, v_1, u_2, v_2$ subject to the constraints (13) and (14). By the Lagrange multiplier method, this can be achieved by solving the system of eight polynomial equations

$$
\begin{aligned}
f_1 &:= \frac{\partial \Delta}{\partial u_0} + \alpha\,\frac{\partial g}{\partial u_0} + \beta\,\frac{\partial h}{\partial u_0} = 0\,, &\quad
f_2 &:= \frac{\partial \Delta}{\partial v_0} + \alpha\,\frac{\partial g}{\partial v_0} + \beta\,\frac{\partial h}{\partial v_0} = 0\,, \\
f_3 &:= \frac{\partial \Delta}{\partial u_1} + \alpha\,\frac{\partial g}{\partial u_1} + \beta\,\frac{\partial h}{\partial u_1} = 0\,, &\quad
f_4 &:= \frac{\partial \Delta}{\partial v_1} + \alpha\,\frac{\partial g}{\partial v_1} + \beta\,\frac{\partial h}{\partial v_1} = 0\,, \\
f_5 &:= \frac{\partial \Delta}{\partial u_2} + \alpha\,\frac{\partial g}{\partial u_2} + \beta\,\frac{\partial h}{\partial u_2} = 0\,, &\quad
f_6 &:= \frac{\partial \Delta}{\partial v_2} + \alpha\,\frac{\partial g}{\partial v_2} + \beta\,\frac{\partial h}{\partial v_2} = 0\,, \\
f_7 &:= g = 0\,, \quad f_8 := h = 0\,.
\end{aligned}
$$

in the real unknowns $u_0, v_0, u_1, v_1, u_2, v_2, \alpha, \beta$ (with α, β being the Lagrange multipliers). Athough the actual values of α, β are of no interest, eliminating them from the system of equations makes it much more complicated.

The Newton–Raphson iteration offers an accurate and efficient approach to solving this system of equations. If $\mathbf{x} = (u_0, v_0, u_1, v_1, u_2, v_2, \alpha, \beta)^T$ is the

vector of unknowns, $\mathbf{M}$ is the corresponding (symmetric) 8×8 Jacobian matrix with elements

$$M_{ij} = \frac{\partial f_i}{\partial x_j}, \quad 1 \leq i, j \leq 8,$$

and $\mathbf{f} = (f_1, f_2, f_3, f_4, f_5, f_6, f_7, f_8)^T$ denotes the vector of function values, the iteration is defined by the relations

$$\mathbf{x}_{k+1} = \mathbf{x}_k + \delta\mathbf{x}_k, \qquad \mathbf{M}_k \, \delta\mathbf{x}_k = -\mathbf{f}_k, \tag{16}$$

the subscripts on $\mathbf{M}$ and $\mathbf{f}$ indicating that they are to be evaluated at $\mathbf{x}_k$. The initial vector $\mathbf{x}_0$ is defined by taking $\alpha = \beta = 1$ and setting

$$\mathbf{w}_0 = u_0 + \mathrm{i}\, v_0 = \sqrt{d_0}\exp(\mathrm{i}\tfrac{1}{2}\theta_0), \quad \mathbf{w}_2 = u_2 + \mathrm{i}\, v_2 = \sqrt{d_1}\exp(\mathrm{i}\tfrac{1}{2}\theta_1),$$

where $d_0 = |\mathbf{d}_0|$, $d_1 = |\mathbf{d}_1|$ and $\theta_0 = \arg(\mathbf{d}_0)$, $\theta_1 = \arg(\mathbf{d}_1)$ are the magnitudes and arguments of the end derivatives $\mathbf{d}_0 = \mathbf{q}'(0) = 5(\mathbf{q}_1 - \mathbf{q}_0)$ and $\mathbf{d}_1 = \mathbf{q}'(1) = 5(\mathbf{q}_5 - \mathbf{q}_4)$ of $\mathbf{q}(t)$, and with these values we take $\mathbf{w}_1 = u_1 + \mathrm{i}\, v_1$ to be the complex root of (7) that yields the smaller value of Δ.

3.2 G^1 PH quintic closest to an ordinary cubic

It may be desirable to guarantee that the PH curve $\mathbf{r}(t)$ matches not only the end points, but also the end tangents, of the prescribed Bézier curve $\mathbf{q}(t)$. With d_0, d_1 and θ_0, θ_1 as defined above in terms of the end derivatives $\mathbf{d}_0, \mathbf{d}_1$ of $\mathbf{q}(t)$ — where $d_0, d_1 > 0$ and $-\pi < \theta_0, \theta_1 \leq \pi$ — we can achieve this by setting $\mathbf{r}'(0) = \mathbf{w}_0^2 = \lambda_0^2\, \mathbf{d}_0$ and $\mathbf{r}'(1) = \mathbf{w}_1^2 = \lambda_1^2\, \mathbf{d}_1$, and hence

$$\mathbf{w}_0 = \lambda_0\sqrt{d_0}\exp(\mathrm{i}\,\tfrac{1}{2}\theta_0), \quad \mathbf{w}_2 = \lambda_1\sqrt{d_1}\exp(\mathrm{i}\,\tfrac{1}{2}\theta_1). \tag{17}$$

The complex variables $\mathbf{w}_0, \mathbf{w}_2$ are thus replaced by the real variables λ_0, λ_1.

With $\mathbf{w}_0, \mathbf{w}_2$ given by (17), the objective function Δ depends on four real variables (λ_0, λ_1 and the real and imaginary parts of $\mathbf{w}_1$), subject to two constraints — the real and imaginary parts of (7). The Lagrange multiplier method yields a system of 6 equations in 6 real unknowns: $u_1, v_1, \lambda_0, \lambda_1$ and the multipliers α, β associated with the real and imaginary parts of (7).

Substituting from (17), setting $\mathbf{w}_1 = u_1 + \mathrm{i}\, v_1$ and

$$(c_0, s_0) := (\cos \tfrac{1}{2}\theta_0, \sin \tfrac{1}{2}\theta_0), \quad (c_1, s_1) := (\cos \tfrac{1}{2}\theta_1, \sin \tfrac{1}{2}\theta_1),$$

the real and imaginary parts of the constraint equation (7) can be written as $g(u_1, v_1, \lambda_0, \lambda_1) = 0$ and $h(u_1, v_1, \lambda_0, \lambda_1) = 0$, with

$$\begin{aligned} g \ := \ & 2\,(u_1^2 - v_1^2) + 3\sqrt{d_0}\lambda_0(c_0 u_1 - s_0 v_1) + 3\sqrt{d_1}\lambda_1(c_1 u_1 - s_1 v_1) \\ & + \ 3\,d_0(c_0^2 - s_0^2)\lambda_0^2 + 3\,d_1(c_1^2 - s_1^2)\lambda_1^2 + \sqrt{d_0 d_1}(c_0 c_1 - s_0 s_1)\lambda_0\lambda_1 - 15\,, \end{aligned}$$

$$\begin{aligned} h \ := \ & 4\,u_1 v_1 + 3\sqrt{d_0}\lambda_0(c_0 v_1 + s_0 u_1) + 3\sqrt{d_1}\lambda_1(c_1 v_1 + s_1 u_1) \\ & + \ 6\,d_0 c_0 s_0\lambda_0^2 + 6\,d_1 c_1 s_1\lambda_1^2 + \sqrt{d_0 d_1}(c_0 s_1 + c_1 s_0)\lambda_0\lambda_1\,. \end{aligned}$$

Similarly, the reduced objective function $\Delta(u_1, v_1, \lambda_0, \lambda_1)$ can be expressed as

$$\begin{aligned} \Delta \ = \ & 2\,d_0^2\,\lambda_0^4 + 2\,d_0^{3/2}\lambda_0^3\,(c_0 u_1 + s_0 v_1) + d_0\,\lambda_0^2\,(u_1^2 + v_1^2) \\ & + \ 2\,d_1^2\,\lambda_1^4 + 2\,d_1^{3/2}\lambda_1^3\,(c_1 u_1 + s_1 v_1) + d_1\,\lambda_1^2\,(u_1^2 + v_1^2) \\ & - \ 10\,[\,a_1\lambda_0^2 + a_2\lambda_1^2 + \sqrt{d_0}\lambda_0(a_3 u_1 - a_4 v_1) + \sqrt{d_1}\lambda_1(a_5 u_1 - a_6 v_1)\,]\,. \quad (18) \end{aligned}$$

with the constants

$$\begin{aligned} a_1 \ = \ & \mathrm{Re}(\mathbf{d}_0(\bar{\mathbf{q}}_1 + \bar{\mathbf{q}}_2))\,, \quad a_2 \ = \ \mathrm{Re}(\mathbf{d}_1(2 - \bar{\mathbf{q}}_3 - \bar{\mathbf{q}}_4))\,, \quad a_3 \ = \ c_0 x_2 + s_0 y_2\,, \\ a_4 \ = \ & s_0 x_2 - c_0 y_2\,, \quad a_5 \ = \ c_1(1 - x_3) - s_1 y_3\,, \quad a_6 \ = \ s_1(1 - x_3) + c_1 y_3\,, \end{aligned}$$

being determined by the control points $\mathbf{q}_k = x_k + \mathrm{i}\,y_k$ of $\mathbf{q}(t)$.

The Lagrange multiplier method then corresponds to solving the system of six polynomial equations

$$\begin{aligned} f_1 \ := \ & \frac{\partial\Delta}{\partial u_1} + \alpha\,\frac{\partial g}{\partial u_1} + \beta\,\frac{\partial h}{\partial u_1} = 0\,, \quad f_2 \ := \ \frac{\partial\Delta}{\partial v_1} + \alpha\,\frac{\partial g}{\partial v_1} + \beta\,\frac{\partial h}{\partial v_1} = 0\,, \\ f_3 \ := \ & \frac{\partial\Delta}{\partial\lambda_0} + \alpha\,\frac{\partial g}{\partial\lambda_0} + \beta\,\frac{\partial h}{\partial\lambda_0} = 0\,, \quad f_4 \ := \ \frac{\partial\Delta}{\partial\lambda_1} + \alpha\,\frac{\partial g}{\partial\lambda_1} + \beta\,\frac{\partial h}{\partial\lambda_1} = 0\,, \\ f_5 \ := \ & g = 0\,, \quad f_6 \ := \ h = 0\,, \end{aligned}$$

in the six real unknowns $u_1, v_1, \lambda_0, \lambda_1, \alpha, \beta$. As before, attempting to directly eliminate the Lagrange multipliers α and β is not advantageous.

To solve the above system by Newton–Raphson iterations, we choose as initial values $\lambda_0 = \lambda_1 = 1$, $\alpha = \beta = 1$, together with the real and imaginary parts of the complex root $\mathbf{w}_1 = u_1 + \mathrm{i}\,v_1$ of (7) — with $\mathbf{w}_0$ and $\mathbf{w}_2$ defined by (17) — that yields the smaller value of Δ. The resulting $\mathbf{w}_0, \mathbf{w}_2$ values define

end derivatives identical to those of the curve being approximated, and the $\mathbf{w}_1$ value ensures satisfaction of the end–point condition (7). To check if the convergence efficiency and consistency depends on the choice $(\alpha, \beta) = (1, 1)$, the Examples below were repeated with $(\alpha, \beta) = (0, 0)$ and $(-1, -1)$. In all of these cases, the same converged solution was obtained, with a number of iterations differing by no more than one.

3.3 G^0 & G^1 PH quintic closest to an ordinary quintic

The approach described in Sections 3.1 and 3.2 for determining the quintic PH curve closest to a given cubic Bézier curve, with G^0 or G^1 end conditions, can also be applied to quintic Bézier curves by simply omitting the degree elevation step that maps (8) into (9). A canonical–form quintic Bézier curve is defined by the four interior control points $\mathbf{q}_1, \mathbf{q}_2, \mathbf{q}_3, \mathbf{q}_4$ while a canonical–form quintic PH curve is effectively defined by just two complex variables — the coefficients $\mathbf{w}_0, \mathbf{w}_1, \mathbf{w}_2$ in (5) subject to the complex constraint (7).

Since the quintic Bézier curve has twice as many free shape parameters as the quintic PH curve, one cannot expect the closest instance of the latter to always be an accurate approximation of the former. Nevertheless, as will be seen in the following examples, an accurate approximation can be possible when the quintic Bézier curve is of relatively simple shape.

4   Computed examples

The methodology described above was implemented using double–precision arithmetic in a `C` language program. The complicated nature of the objective functions and constraints that identify closest G^0 and G^1 quintic PH curves precludes a rigorous analysis of the number and nature of the extrema that the optimization problem admits. Consequently, this issue was investigated empirically for several test cases by starting the Newton–Raphson iterations from points on a rectangular array of values $u_0, v_0, u_1, v_1, u_2, v_2, \alpha, \beta$ (for G^0) and $u_1, v_1, \lambda_0, \lambda_1, \alpha, \beta$ (for G^1), with each variable in the interval $[-2, 2]$. It was found that, whenever the procedure converged in a reasonable number of iterations, the resulting values correspond to a *unique* solution.

As evident from the examples below, the initial values of the optimization variables proposed in Section 3 yield rapid convergence (with between 4 and 9 Newton–Raphson iterations) to the unique solution. To assess the agreement

of the closest PH quintic $\mathbf{r}(t)$ with a prescribed cubic or quintic Bézier curve $\mathbf{q}(t)$, the following two root–mean–square measures are used:

$$e = \left[\frac{1}{6} \sum_{k=0}^{5} |\mathbf{p}_k - \mathbf{q}_k|^2 \right]^{1/2} \quad \text{and} \quad \epsilon = \left[\int_0^1 |\mathbf{r}(t) - \mathbf{q}(t)|^2 \, \mathrm{d}t \right]^{1/2}. \quad (19)$$

We note that $e = 0$ when $\mathbf{q}(t)$ is itself a (possibly degree–elevated) PH curve. However, the quantity ϵ depends on not only on the loci of $\mathbf{q}(t)$ and $\mathbf{r}(t)$, but also on their parametrizations.

4.1 Quintic PH curve closest to a cubic Bézier curve

Example 1. Consider the canonical–form cubic Bézier curve defined by the control points

$$\mathbf{c}_0 = 0.0 + 0.0\,\mathrm{i}, \quad \mathbf{c}_1 = 0.3 + 0.5\,\mathrm{i}, \quad \mathbf{c}_2 = 0.8 + 0.7\,\mathrm{i}, \quad \mathbf{c}_3 = 1.0 + 0.0\,\mathrm{i}.$$

The G^0 PH quintic converges in 5 Newton–Raphson iterations with a value $\Delta = 1.0 \times 10^{-14}$ of (15), and the converged values are

$$
\begin{aligned}
(u_0, v_0) &= (1.197306, 0.675613), \\
(u_1, v_1) &= (0.974560, 0.228594), \\
(u_2, v_2) &= (1.134403, -0.922940),
\end{aligned}
$$

with $(\alpha, \beta) = (0.023645, -0.054670)$ and values $e = 0.023527$, $\epsilon = 0.007428$ for the quantities (19). The G^1 PH quintic converges in 4 Newton–Raphson iterations with a value $\Delta = 9.0 \times 10^{-15}$ of (18), and the converged values are

$$
\begin{aligned}
(u_1, v_1) &= (0.907606, 0.182606), \\
(\lambda_0, \lambda_1) &= (1.056574, 0.991821),
\end{aligned}
$$

with $(\alpha, \beta) = (0.027887, -0.077594)$ and values $e = 0.028602$, $\epsilon = 0.012908$ for the quantities (19). The end point condition (7) is satisfied to an accuracy of 10^{-15} for both the G^0 quintic and the G^1 PH quintic.

Figure 1 compares the G^0 and G^1 PH quintics closest to the cubic Bézier curve. Although both are seen to closely approximate the given cubic curve, the G^0 case conforms somewhat more closely to it than the G^1 case, since it incorporates more free optimization parameters.
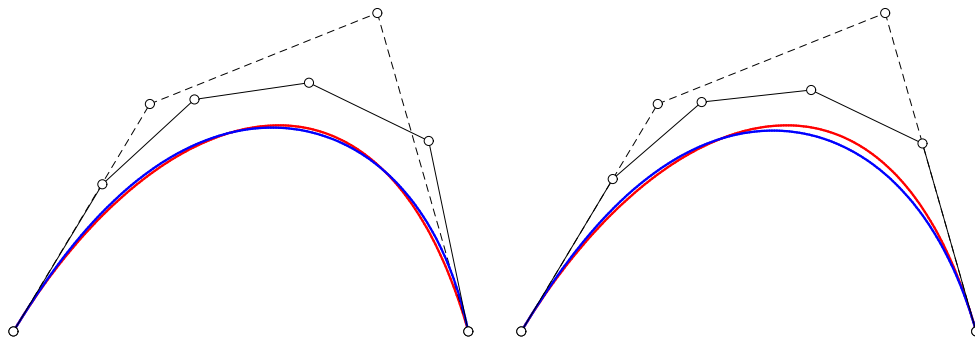
11

Figure 1: G^0 (left) and G^1 (right) quintic PH curves (blue with solid control polygons) closest to a given "ordinary" cubic Bézier curve (red with dashed control polygon) for the curve data in Example 1.

Figure 2 shows the C^1 PH quintic Hermite interpolant to the end points and end derivatives of the ordinary cubic Bézier curve. It is evident that the closest G^0 and G^1 quintic PH curves are better approximants to the cubic — for the PH quintic Hermite interpolant, the quantities (19) have the values $e = 0.038276$ and $\epsilon = 0.026267$.
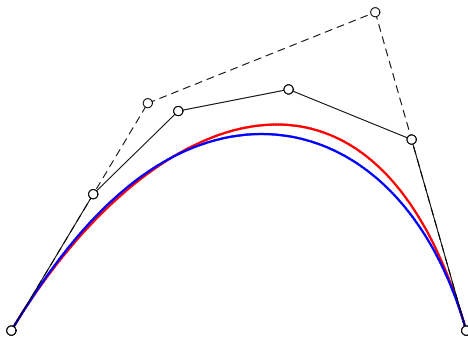
Figure 2: The PH quintic Hermite interpolant (blue & solid control polygon) to the end points and end derivatives of the "ordinary" cubic Bézier curve (red & dashed control polygon) in Example 1 — compare with Figure 1.

Example 2. Consider the canonical–form inflectional cubic Bézier curve specified by the control points

$$\mathbf{c}_0 = 0.0 + 0.0\,\mathrm{i}\,, \quad \mathbf{c}_1 = 0.4 + 0.5\,\mathrm{i}\,, \quad \mathbf{c}_2 = 0.7 - 0.4\,\mathrm{i}\,, \quad \mathbf{c}_3 = 1.0 + 0.0\,\mathrm{i}\,.$$

The G^0 PH quintic converges in 7 Newton–Raphson iterations with a value $\Delta = 1.2 \times 10^{-14}$ of (15), and the converged values are

$$
\begin{aligned}
(u_0, v_0) &= (1.133397, 0.575159) \,, \\
(u_1, v_1) &= (0.969059, -1.043523) \,, \\
(u_2, v_2) &= (0.975987, 0.455088) \,,
\end{aligned}
$$

with $(\alpha, \beta) = (-0.104502, 0.164942)$ and values $e = 0.062425$, $\epsilon = 0.019455$ for the quantities (19). The G^1 PH quintic converges in 5 Newton–Raphson iterations with a value $\Delta = 3.0 \times 10^{-15}$ of (18), and the converged values are

$$
\begin{aligned}
(u_1, v_1) &= (0.969380, -1.042813) \,, \\
(\lambda_0, \lambda_1) &= (0.915851, 0.878917) \,,
\end{aligned}
$$

with $(\alpha, \beta) = (-0.104838, 0.168749)$ and values $e = 0.063724$, $\epsilon = 0.021806$ for the quantities (19). The end point condition (7) is satisfied to an accuracy of 10^{-15} for both the G^0 quintic and the G^1 PH quintic.
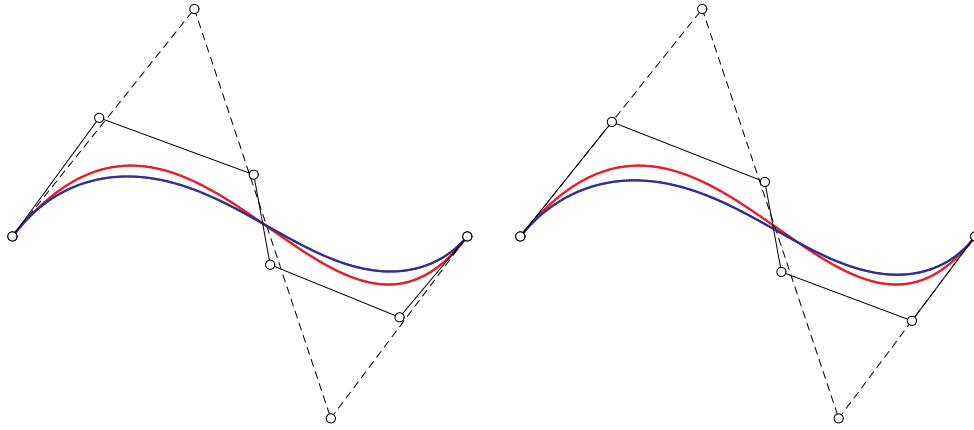

Figure 3: G^0 (left) and G^1 (right) quintic PH curves (blue with solid control polygons) closest to a given "ordinary" cubic Bézier curve (red with dashed control polygon) for the curve data in Example 2.

Figure 3 compares the G^0 and G^1 PH quintics closest to the cubic Bézier curve. In this case the PH quintics are not as close as in Example 1, because of the stronger curvature variation of the cubic curve (the G^0 case conforms more closely to the cubic than the G^1 case). Figure 4 shows the PH quintic

Hermite interpolant to the end points and end derivatives of the cubic Bézier curve. This has values $e = 0.078544$ and $\epsilon = 0.019839$, similar to the closest G^0 and G^1 PH quintics, but it is quite "flat" over much of its extent.
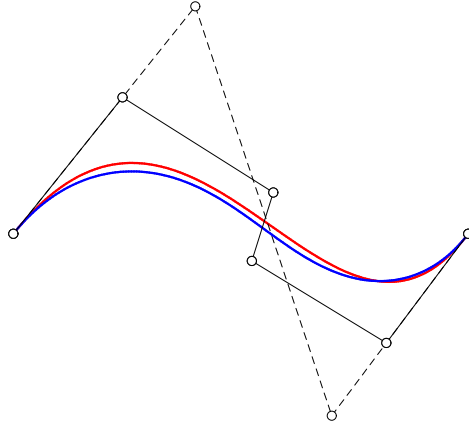

Figure 4: The PH quintic interpolant (blue with solid control polygon) to the end points and end derivatives of the "ordinary" cubic Bézier curve (red with dashed control polygon) in Example 1 — compare with Figure 3.

Examples 1 and 2 highlight two noteworthy points: (1) quintic PH curves exhibit more moderate curvature variations than "ordinary" cubic curves [5]; and (2) consequently, the closest PH quintics offer better approximants to convex cubic segments than to inflectional segments.

4.2 Quintic PH curve closest to a quintic Bézier curve

The following examples illustrate application of the method to quintic Bézier curves. As noted in Section 3.3, quintic PH curves have only half the number of shape freedoms of ordinary quintic Bézier curves, so one cannot expect the closest PH quintic to conform as closely as in the case of cubic Bézier curves.

Example 3. Consider the canonical–form quintic Bézier curve specified by the control points

$$\mathbf{q}_0 = 0.0 + 0.0\,\mathrm{i}\,, \quad \mathbf{q}_1 = 0.2 + 0.5\,\mathrm{i}\,, \quad \mathbf{q}_2 = 0.4 + 0.7\,\mathrm{i}\,,$$
$$\mathbf{q}_3 = 0.6 + 0.7\,\mathrm{i}\,, \quad \mathbf{q}_4 = 0.8 + 0.5\,\mathrm{i}\,, \quad \mathbf{q}_5 = 1.0 + 0.0\,\mathrm{i}\,.$$

The G^0 quintic PH curve converges in 6 Newton–Raphson iterations with a value $\Delta = 1.6 \times 10^{-14}$, with the end point condition (7) satisfied to an accuracy of 10^{-15}. The converged values of the solution variables are

$$\begin{aligned}
(u_0, v_0) &= (1.362842, 0.973626), \\
(u_1, v_1) &= (0.703134, 0.000000), \\
(u_2, v_2) &= (1.362842, -0.973626),
\end{aligned}$$

with $(\alpha, \beta) = (0.122923, 0.000000)$ and values $e = 0.031728$, $\epsilon = 0.010500$ for the quantities (19). The symmetry of the solution values, and the fact that $v_1 = \text{Im}(\mathbf{w}_1) = 0$, reflect the symmetry of the input curve.

The G^1 PH quintic converges in just 4 Newton–Raphson iterations with $\Delta = 2.6 \times 10^{-14}$, the end point condition (7) being satisfied to an accuracy of 10^{-15}. The converged values of the solution variables are

$$\begin{aligned}
(u_1, v_1) &= (0.596699, 0.000000), \\
(\lambda_0, \lambda_1) &= (1.032426, 1.032426)
\end{aligned}$$

with $(\alpha, \beta) = (0.144813, 0.000000)$ and the values of the quantities (19) are $e = 0.038816$ and $\epsilon = 0.012998$.
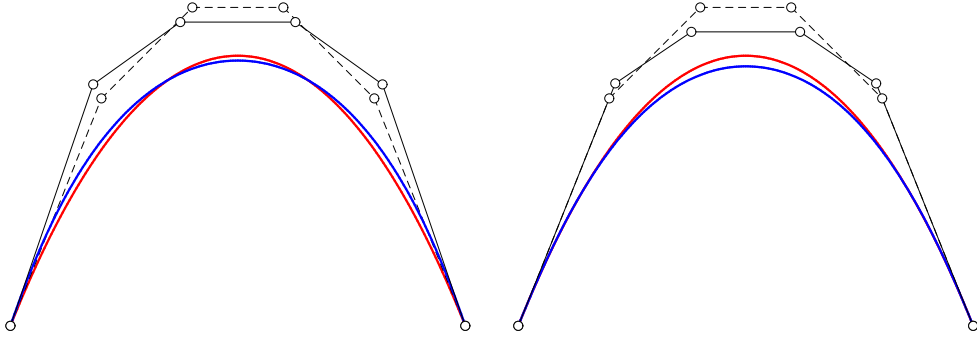

Figure 5: G^0 (left) and G^1 (right) quintic PH curves (blue with solid control polygons) closest to a given "ordinary" quintic Bézier curve (red with dashed control polygon) for the curve data in Example 3.

Figure 5 illustrates the G^0 and G^1 quintic PH curves closest to the given "ordinary" quintic Bézier curve. As with the cubic Bézier curves, the closest quintic PH curves are much better approximants than the PH quintic Hermite interpolant matching the end points and end derivatives of the Bézier curve.

Example 4. As previously noted, quintic Bézier curves have twice as many free shape parameters as quintic PH curves, so the quintic PH curve closest to a given quintic Bézier curve may not always be a reasonable approximation of it. In the preceding example, a good approximation was possible because of the simple convex nature of the quintic Bézier curve. We now investigate a more challenging case, defined by the control points

$$\mathbf{q}_0 = 0.0 + 0.0\,\mathrm{i}\,, \quad \mathbf{q}_1 = 0.2 + 0.5\,\mathrm{i}\,, \quad \mathbf{q}_2 = 0.4 + 0.7\,\mathrm{i}\,,$$
$$\mathbf{q}_3 = 0.6 - 0.7\,\mathrm{i}\,, \quad \mathbf{q}_4 = 0.8 - 0.5\,\mathrm{i}\,, \quad \mathbf{q}_5 = 1.0 + 0.0\,\mathrm{i}\,.$$

As seen in Figure 6, this defines an inflectional curve with a strong curvature variation. The closest G^0 and G^1 PH quintics converge in 9 and 5 iterations, with $\Delta = 4.3 \times 10^{-14}$ and $\Delta = 7.0 \times 10^{-15}$. The corresponding quantities (19) have the rather large values: $e = 0.285506$, $\epsilon = 0.120531$ and $e = 0.350921$, $\epsilon = 0.128283$. Figure 6 illustrates the G^0 and G^1 quintic PH curves closest to the given quintic Bézier curve. The limitations of approximating a Bézier curve by a PH curve with fewer shape freedoms are clearly apparent.
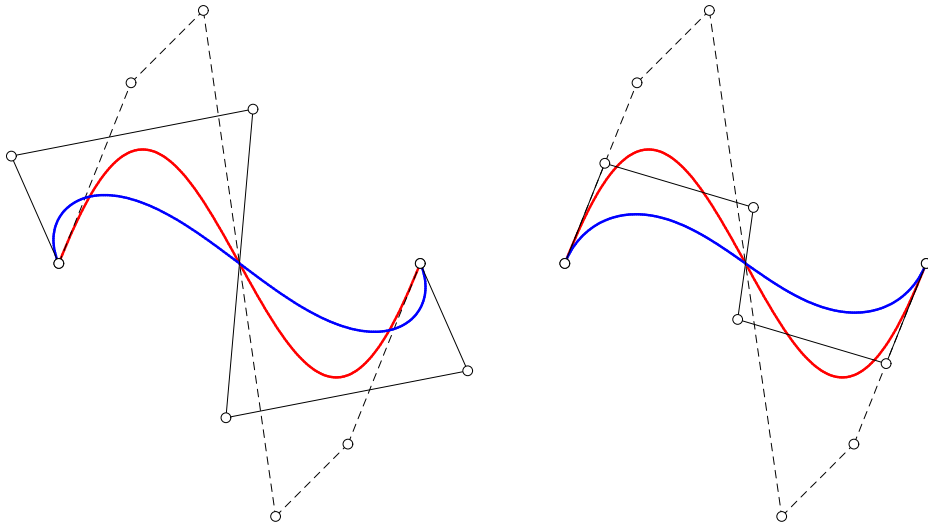

Figure 6: G^0 (left) and G^1 (right) quintic PH curves (blue with solid control polygons) closest to a given "ordinary" quintic Bézier curve (red with dashed control polygon) for the curve data in Example 4.

One way to address this limitation in identifying the closest PH curve to a prescribed Bézier of equal degree is to subdivide the latter into segments

16

with simpler curvature variation, and apply the method to the subsegments individually. Figure 7 shows the result of this approach upon subdividing the quintic Bézier curve at the inflection point, and a substantial improvement over the results shown in Figure 6 is evident.
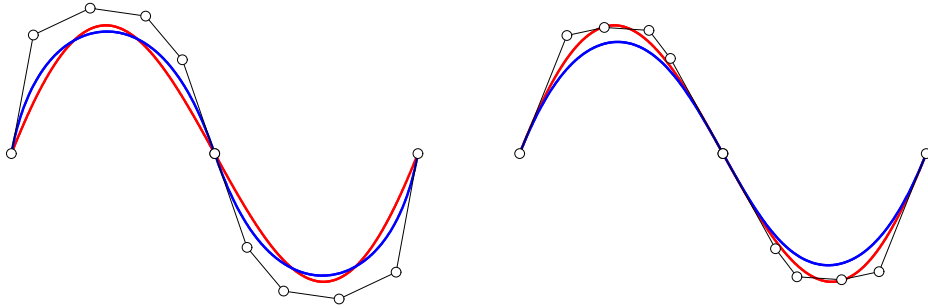

Figure 7: G^0 (left) and G^1 (right) quintic PH curves (blue with solid control polygons) closest to an "ordinary" quintic Bézier curve (red, control polygon not shown) for the data in Example 4 after subdivision at the inflection point.

However it is preferable to seek the closest PH curve whose degree admits a number of shape freedoms not less than that of the prescribed Bézier curve. For an odd degree n, a canonical–form Bézier curve is characterized by $n-1$ complex values, while a PH curve is characterized by $m = \frac{1}{2}(n-1)$ complex values — the pre–image polynomial $\mathbf{w}(t)$ possesses $m+1$ complex coefficients $\mathbf{w}_0, \ldots, \mathbf{w}_m$ subject to a generalization of the end–point constraint (7). This yields a coincidence in the number of shape freedoms for Bézier cubics and PH quintics, but for Bézier quintics we must proceed to degree 9 PH curves in order to secure the same number of shape freedoms.

Example 5. As a final example, we modify a quintic PH curve by perturbing a single control point so that the perturbed curve is no longer a PH curve, as shown in Figure 8. We then determine the G^0 quintic PH curve closest to the modified curve. The Newton–Raphson scheme converges in 6 iterations, with values $e = 0.101439$ and $\epsilon = 0.032522$ for the quantities (19). A closer approximation can be obtained by identifying the degree 7 PH curve closest to the quintic Bézier curve obtained from the modified quintic PH curve.

It is noteworthy that, in all the above examples, the measures (19) satisfy $e > \epsilon$. This may be viewed as a consequence of the fact that the Bézier control polygon "exaggerates" the shape of a curve. Consequently, the measure e of
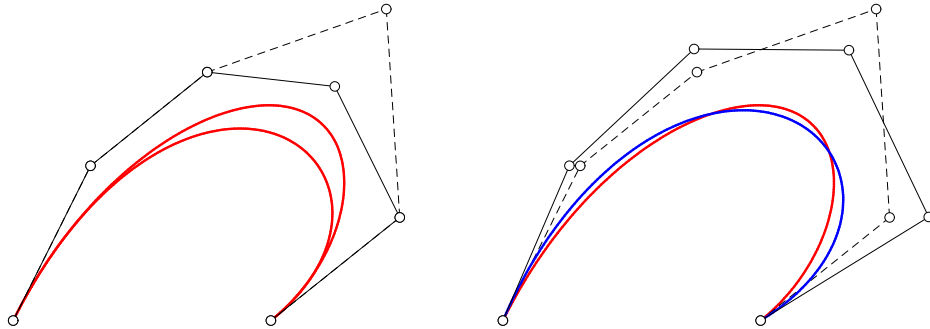
Figure 8: Left: a quintic PH curve (solid polygon) modified by displacement of a single control point (dashed polygon). Right: the PH quintic (blue) that is closest to the modified curve (red) — which is no longer a PH curve.

the discrepancy between the control points of two similar curves is generally expected to exceed the integral measure ϵ of the deviation of corresponding points (as defined by their parameterizations) on their loci.

5 Extensions and generalizations

The principles developed herein for identifying quintic PH curves closest to given Bézier curves can be readily generalized to higher–degree PH curves. The basic approach remains the same, although the objective functions and constraints, being dependent on more free parameters, become more involved. We now briefly outline some other possible extensions of the methodology (for brevity, the discussion is couched in the context of quintic PH curves).

5.1 Arc length constraints

For a planar quintic PH curve to have a specified arc length L, the coefficients of the quadratic complex polynomial (5) must [6] satisfy the condition

$$2\,|\mathbf{w}_1|^2 + 3\,\mathrm{Re}((\overline{\mathbf{w}}_0 + \overline{\mathbf{w}}_2)\mathbf{w}_1) + 3\,|\mathbf{w}_0|^2 + 3\,|\mathbf{w}_2|^2 + \mathrm{Re}(\overline{\mathbf{w}}_0\mathbf{w}_2) \;=\; 15\,L\,,$$

which may be expressed (in the G^1 case) in terms of $u_1, v_1, \lambda_0, \lambda_1$ through the relations $\mathbf{w}_1 = u_1 + \mathrm{i}\,v_1$ and (17). To force the quintic PH curve to have the same arc length L as a given ordinary cubic curve,[2] this condition must

_____

[2]Note that L must be computed by numerical quadrature.

18

be introduced as a constraint with an associated Lagrange multiplier γ. The optimization problem then incurs a system of 7 equations in 7 real unknowns.

5.2 Imposing G^2 end conditions

The end–point curvatures of a quintic PH curve are

$$\kappa_0 = 4\,\frac{\mathrm{Im}(\overline{\mathbf{w}}_0\mathbf{w}_1)}{|\mathbf{w}_0|^4} = 4\,\lambda_0\sqrt{d_0}\,(c_0v_1 - s_0u_1)\,,$$

$$\kappa_1 = 4\,\frac{\mathrm{Im}(\overline{\mathbf{w}}_1\mathbf{w}_2)}{|\mathbf{w}_2|^4} = 4\,\lambda_1\sqrt{d_1}\,(s_1u_1 - c_1v_1)\,.$$

These equations may be regarded as specifying λ_0, λ_1 in terms of the known quantities d_0, c_0, s_0, κ_0 and d_1, c_1, s_1, κ_1, leaving only u_1, v_1 as free variables. Since the end–point condition for a canonical–form PH quintic (amounting to two scalar constraints) must still be satisfied, there are no remaining free parameters. It is therefore necessary to employ higher–order PH curves when G^2 end conditions are imposed. The G^2 interpolation problem using degree 7 PH curves, including an arc length constraint, is discussed in [13].

5.3 Extension to spatial PH curves

A spatial PH quintic curve $\mathbf{r}(t)$ may be generated from a quadratic quaternion polynomial

$$\mathcal{A}(t) = \mathcal{A}_0(1 - t)^2 + \mathcal{A}_1 2(1 - t)t + \mathcal{A}_2 t^2 \tag{20}$$

by integrating $\mathbf{r}'(t) = \mathcal{A}(t)\,\mathbf{i}\,\mathcal{A}^*(t)$, where $\mathcal{A}^*(t)$ is the conjugate of $\mathcal{A}(t)$. The control points of $\mathbf{r}(t)$ are then specified by

$$\mathbf{p}_1 = \mathbf{p}_0 + \frac{1}{5}\mathcal{A}_0\,\mathbf{i}\,\mathcal{A}_0^*\,,$$

$$\mathbf{p}_2 = \mathbf{p}_1 + \frac{1}{10}\left(\mathcal{A}_0\,\mathbf{i}\,\mathcal{A}_1^* + \mathcal{A}_1\,\mathbf{i}\,\mathcal{A}_0^*\right)\,,$$

$$\mathbf{p}_3 = \mathbf{p}_2 + \frac{1}{30}\left(\mathcal{A}_0\,\mathbf{i}\,\mathcal{A}_2^* + 4\,\mathcal{A}_1\,\mathbf{i}\,\mathcal{A}_1^* + \mathcal{A}_2\,\mathbf{i}\,\mathcal{A}_0^*\right)\,,$$

$$\mathbf{p}_4 = \mathbf{p}_3 + \frac{1}{10}\left(\mathcal{A}_1\,\mathbf{i}\,\mathcal{A}_2^* + \mathcal{A}_2\,\mathbf{i}\,\mathcal{A}_1^*\right)\,,$$

$$\mathbf{p}_5 = \mathbf{p}_4 + \frac{1}{5}\mathcal{A}_2\,\mathbf{i}\,\mathcal{A}_2^*\,. \tag{21}$$

For a canonical–form curve with $\mathbf{r}(0) = (0,0,0)$ and $\mathbf{r}(1) = (1,0,0)$ we choose $\mathbf{p}_0 = 0$, and setting $\mathbf{r}(1) = \mathbf{p}_5 = \mathbf{i}$ imposes the (vector) quadratic condition

$$
\begin{aligned}
6\,\mathcal{A}_0\,\mathbf{i}\,\mathcal{A}_0^* &+ 3\,(\mathcal{A}_0\,\mathbf{i}\,\mathcal{A}_1^* + \mathcal{A}_1\,\mathbf{i}\,\mathcal{A}_0^*) \\
+\ \mathcal{A}_0\,\mathbf{i}\,\mathcal{A}_2^* &+ 4\,\mathcal{A}_1\,\mathbf{i}\,\mathcal{A}_1^* + \mathcal{A}_2\,\mathbf{i}\,\mathcal{A}_0^* \\
+\ 3\,(\mathcal{A}_1\,\mathbf{i}\,\mathcal{A}_2^* &+ \mathcal{A}_2\,\mathbf{i}\,\mathcal{A}_2^*) + 6\,\mathcal{A}_2\,\mathbf{i}\,\mathcal{A}_2^* \ =\ 30\,\mathbf{i}
\end{aligned}
\tag{22}
$$

on the coefficients of $\mathcal{A}(t)$. For a given canonical–form ordinary quintic space curve $\mathbf{q}(t)$ with control points $\mathbf{q}_0, \ldots, \mathbf{q}_5$ we want to identify the coefficients $\mathcal{A}_0, \mathcal{A}_1, \mathcal{A}_2$ that minimize the quantity

$$
\Delta \ = \ \sum_{k=0}^{5} |\mathbf{p}_k - \mathbf{q}_k|^2 \,.
$$

while satisfying (22). The coefficients of (20) incorporate 12 scalar variables, and 3 Lagrange multipliers must be associated with the (x, y, z) components of the vector constraint (22). Hence, for the G^0 case, the minimization of Δ incurs a system of 15 equations in 15 unknowns. However, in the G^1 case, $\mathcal{A}_0$ and $\mathcal{A}_2$ will each depend on only two scalar variables.

5.4 Extension to PH spline curves

The construction of a planar C^2 PH quintic spline curves that interpolate a given sequence of points was described in [2], and the determination of its B–spline control polygon was formulated in [8]. As observed in [1], PH spline curves can be defined directly in terms of the B–spline form, and the problem of finding the PH spline that most closely approximates a given "ordinary" spline curve can be formulated in terms of minimizing the sum of the squared differences of their control points. This incurs objective functions dependent on many variables, and may be computationally expensive. An alternative is to extract the individual B–spline curve segments as Bézier curves and apply the approach described herein, with G^1 (or possibly G^2) end conditions.

6 Closure

By expressing the sum of squared differences between the control points of a given planar Bézier and those of a planar PH curve in terms of the coefficients

of the complex PH curve pre–image polynomial, the task of identifying the PH curve "closest" to the Bézier curve can be formulated as a constrained polynomial optimization problem. Invoking the Lagrange multiplier method, this problem can be efficiently solved to machine precision by a few Newton–Raphson iterations. This offers a novel route to importing PH curves to CAD systems, as an alternative to the Hermite and spline interpolation schemes that are commonly employed to construct PH curves.

The "closest" PH curves are constructed so as to possess the same end points (or end points and end tangents) as the given Bézier curve. Although the focus herein was on quintic PH curves, the methodology can be readily adapted to higher degree PH curves. Quintic PH curves are found to closely approximate cubic Bézier curves, with which they possess the same number of shape freedoms. Examples of the approximation of quintic Bézier curves by quintic PH curves (with fewer shape freedoms) were also presented. Close approximations can be achieved for curves without severe curvature variation — otherwise, subdivision methods can be used to improve the accuracy.

A number of extensions and generalizations of the methodology were also briefly discussed, including imposition of arc length constraints or G^2 end conditions; adaptation to spatial PH curves based on the quaternion form; and the extension to PH spline curves. Another possibility is the application to PH curves constructed in more general function spaces [24].

References

[1] G. Albrecht, C. V. Beccari, J–C. Canonne, and L. Romani (2017), Planar Pythagorean–hodograph B–spline curves, *Comput. Aided Geom. Design* **57**, 57–77.

[2] G. Albrecht and R. T. Farouki (1996), Construction of C^2 Pythagorean–hodograph interpolating splines by the homotopy method, *Adv. Comp. Math.* **5**, 417–442.

[3] H. I. Choi and H. P. Moon (2008), Weierstrass–type approximation theorem with Pythagorean–hodograph curves, *Comput. Aided Geom. Design* **25**, 305–319.

[4] R. T. Farouki (1994), The conformal map $z \rightarrow z^2$ of the hodograph plane, *Comput. Aided Geom. Design* **11**, 363–390.

[5] R. T. Farouki (2008), *Pythagorean–Hodograph Curves: Algebra and Geometry Inseparable*, Springer, Berlin.

[6] R. T. Farouki (2016), Construction of G^1 planar Hermite interpolants with prescribed arc lengths, *Comput. Aided Geom. Design* **46**, 64–75.

[7] R. T. Farouki (2019), Existence of Pythagorean–hodograph quintic interpolants to spatial G^1 Hermite data with prescribed arc lengths, *J. Symb. Comput.* **95**, 202–216.

[8] R. T. Farouki, C. Giannelli, and A. Sestini (2016), Local modification of Pythagorean–hodograph quintic spline curves using the B–spline form, *Adv. Comp. Math.* **42**, 199–225.

[9] R. T. Farouki, C. Giannelli, and A. Sestini (2019), New developments in theory, algorithms, and applications for Pythagorean–hodograph curves, *Advanced Methods for Geometric Modeling and Numerical Simulation* (C. Giannelli and H. Speleers, eds.), Springer, ISBN 978–3–030–27331–6, pp. 127–177.

[10] R. T. Farouki, C. Giannelli, C. Manni, and A. Sestini (2008), Identification of spatial PH quintic Hermite interpolants with near–optimal shape measures, *Comput. Aided Geom. Design* **25**, 274–297.

[11] R. T. Farouki, B. K. Kuspa, C. Manni, and A. Sestini (2001), Efficient solution of the complex quadratic tridiagonal system for C^2 PH quintic splines, *Numer. Algor.* **27**, 35–60.

[12] R. T. Farouki and C. A. Neff (1995), Hermite interpolation by Pythagorean–hodograph quintics, *Math. Comp.* **64**, 1589–1609.

[13] R. T. Farouki, F. Pelosi, and M. L. Sampoli (2021), Approximation of monotone clothoid segments by degree 7 Pythagorean–hodograph curves, *J. Comput. Appl. Math.* **382**, article 113110.

[14] R. T. Farouki and T. Sakkalis (1990), Pythagorean hodographs, *IBM J. Res. Develop.* **34**, 736–752.

[15] G. Jaklič, J. Kozak, M. Krajnc, V. Vitrih, and E. Žagar (2010), On interpolation by planar G^2 Pythagorean–hodograph spline curves, *Math. Comp.* **79**, 305–326.

[16] B. Jüttler (2001), Hermite interpolation by Pythagorean hodograph curves of degree seven, *Math. Comp.* **70**, 1089–1111.

[17] S. H. Kim and H. P. Moon (2017), Rectifying control polygon for planar Pythagorean hodograph curves, *Comput. Aided Geom. Design* **54**, 1–14.

[18] S. H. Kim and H. P. Moon (2019), Gauss–Lobatto polygon of Pythagorean hodograph curves, *Comput. Aided Geom. Design* **74**, article 101768.

[19] J. Kosinka and M. Lavicka (2014), Pythagorean hodograph curves: A survey of recent advances, *J. Geom. Graphics* **18**, 23–34.

[20] K. K. Kubota (1972), Pythagorean triples in unique factorization domains, *Amer. Math. Monthly* **79**, 503–505.

[21] S. H. Kwon (2010), Solvability of G^1 Hermite interpolation by spatial Pythagorean–hodograph cubics and its selection scheme, *Comput. Aided Geom. Design* **27**, 138–149.

[22] H. P. Moon, S. H. Kim, and S. H. Kwon (2020), Controlling extremal Pythagorean hodograph curves by Gauss–Legendre polygons, *Comput. Aided Geom. Design* **80**, article 101852.

[23] F. Pelosi, M. L. Sampoli, R. T. Farouki, and C. Manni (2007), A control polygon scheme for design of planar C^2 PH quintic spline curves, *Comput. Aided Geom. Design* **24**, 28–52.

[24] L. Romani, L. Saini, and G. Albrecht (2014), Algebraic–trigonometric Pythagorean–hodograph curves and their use for Hermite interpolation. *Adv. Comp. Math.* **40**, 977–1010.

[25] Z. Šir and B. Jüttler (2007), C^2 Hermite interpolation by Pythagorean hodograph space curves, *Math. Comp.* **76**, 1373–1391.

[26] D. R. Smith (1974), *Variational Methods in Optimization*, Dover Publications (reprint), Mineola, New York.